



Influence of Geocell Reinforcement on Bearing Capacity of Low-Volume Roads

Jose Luis Arias¹ · Sundeep Inti² · Vivek Tandon³

Received: 3 December 2017 / Accepted: 6 January 2020 / Published online: 5 February 2020
© Springer Nature Switzerland AG 2020

Abstract

This study examined the working principles of the geocell reinforcement in low-volume roads through laboratory testing and finite-element modeling (FEM). A steel box of 1.5 m × 1.2 m × 0.9 m (5 ft. × 4 ft. × 3 ft.) was fabricated to accommodate multiple pavement layers. A quarter of the laboratory test box was modeled using commercially available FEM software. A low modulus base and subgrade materials were selected, and the base layer was reinforced with 152 mm (6 in.) high geocell to evaluate the benefits of geocell reinforcement. A dynamic cyclic load of 551 kPa (80 psi) was applied for a set number of cycles (20,000 in the laboratory and 100 during computer simulations). The laboratory test setup was instrumented to record the responses of the material under dynamic cyclic loading. Since the transducers generated substantial data points along with associated signal noise, a set of procedures were incorporated to minimize the electronic noise and reduce the data size. The laboratory test results indicated that the geocell-reinforced sections experienced lower vertical stresses imparted on top of the subgrade nearly by 30% in comparison to unreinforced sections. The vertical pressure distribution beneath the geocell layer suggests that the reinforcement is acting like a combination of flexible and rigid pavement. The geocell-reinforced layer performed well even with an increase in stresses from 689 kPa (100 psi) to 827 kPa (120 psi). Although similar hoop strains trends were observed, the hoop strains estimated from FEM were different than the ones measured in the laboratory.

Keywords Geocell working principles · Low-volume roads · Finite-element modeling

Introduction

Geocell reinforcement paved the way for using locally available inferior materials in the road construction. Geocell is an interconnection of cells that form a honeycomb pattern, which provides confinement to the inferior material and laterally distributes the load. It reduces the load transferred to the layer below (subgrade layer). When a load is applied, the geocell reinforcement holds the infill material in cells from being displaced by hoop action in the cell walls, thereby

increasing the shear strength of the composite system [1]. In addition to the hoop action, the surrounding cells provide passive resistance, and friction offered by geocell wall and infill material further contribute towards the reduction of stress, thus, increasing the bearing capacity of the layer beneath the geocell-reinforced layer [2]. In unpaved roads, the geocell reinforces the unbound aggregates and reduces the deformation. The geocell reinforcement aids in reducing the thickness of the base layers [3, 4]. In unpaved and low-volume roads, a significant amount of traffic load is carried by the base layers, which requires either a thicker base layer or a high strength base material. Geocell is believed to be a suitable alternative for the low-volume roads, because it reduces the need for a thicker base layer or high-quality base materials.

Numerous studies were performed in the past decade on the geocell reinforcement. These studies can be classified as employing the geocell as a building foundation support [1, 5–12], railroad subgrade or base improvement [13–17], and base or subgrade improvement in roads [18–28]. All these studies documented the benefit of

✉ Vivek Tandon
vivek@utep.edu

¹ TBPE Firm Registration No. F10632, CQC Testing and Engineering, L.L.C, 4606 Titanic Avenue, El Paso, TX 79904, USA

² Department of Construction Science and Organizational Leadership, College of Technology, Purdue Northwest University, Westville, IN 46391, USA

³ Department of Civil Engineering, The University of Texas at El Paso, 500 W. Uni. Ave., El Paso, TX 79968, USA

geocell and its working principles. However, there were limited studies on designing roads with geocell reinforcement. Pokharel (2010) developed a design method using geocell for low-volume roads with no surface layers, which were a modification of unpaved roads design with planar geosynthetics [29]. The proposed model was based on limited test data (geocell from one manufacturer and four base materials), and its applicability on a different type of material (other than tested) is questionable. The other available design method was developed by Presto Geosystem (2008), in which the main design criterion is the friction angle between the infill and geocell wall. The proposed method does not consider the quality of infill material in the geocell and is based solely on the type of material sand, silt, and stone. Recent studies [2, 3] worked towards the design methods. However, the proposed models are either not based on extensive laboratory tests or field studies.

Developing a design method for low-volume roads needs robust laboratory testing, numerical analysis, parametric study, and refined quality data. The primary objective of this study is to present laboratory testing, refinement of the laboratory data, and calibration and validation of the developed FEM model. Also, this study evaluated the working principles of geocell. This manuscript provides useful information to the blooming researchers in developing the lab as well as FEM modeling. The detailed discussion on the laboratory evaluation and FEM is included in the following sections.

Test Setup and FEM

Since the purpose of this study is to perform groundwork for the design, a laboratory test setup is developed along with representative FEM. Therefore, the laboratory test setup and FEM had similar dimensions and boundary conditions.

Laboratory Setup

A rectangular steel tank 1.5 m × 1.2 m × 0.9 m was fabricated to simulate a field pavement section in the laboratory, as shown in the schematic in Fig. 1a. This tank can accommodate multiple pavement layers (subgrade, geocell-reinforced or geocell-unreinforced base layer, and a base layer on top as a cover). The length and width of the box were chosen based on the preliminary study with a focus to minimize the influence of the box boundary on the measured test results and considering the typical geocell sizes available for reinforcement.

A height of 915 mm was chosen to accommodate 610 mm of subgrade and 305 mm of base layers. The base layer thickness was selected based on the height of the geocell available in the market and the recommended cover thickness (by geocell manufacturers and researchers), and typical base thickness used in low-volume roads within Texas. The commonly available geocell sizes are 76, 100, 150, and 200 mm. Even though manufacturers recommended a minimum cover thickness of 50 mm, the published literature [7–9] suggests the use of cover thickness ranging from 25 to 152 mm for various applications.

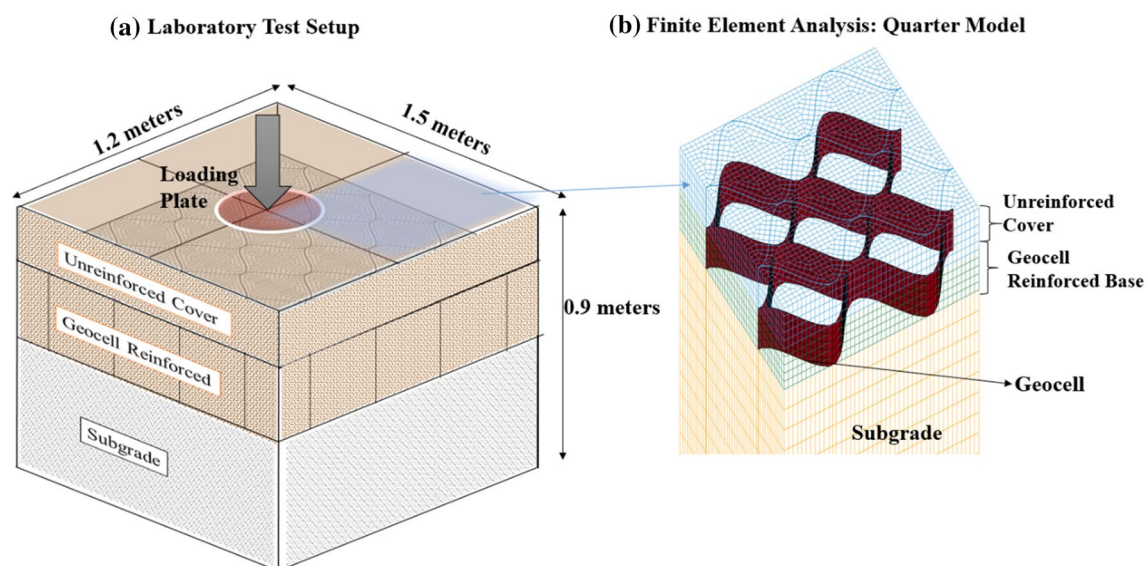


Fig. 1 a Laboratory setup and b FEM quarter model

By considering the combination of geocell and cover thickness, the maximum anticipated base layer thickness will be 305 mm.

Once the base layer thickness is selected, a preliminary pavement analysis was performed to evaluate the vertical stress distribution in the subgrade using the linear elastic multi-layer model (BISAR [37]). In the analysis, various combinations of base modulus and thicknesses, and subgrade modulus were used. The results indicated that even for the weaker base and subgrade modulus, the vertical stresses in subgrade faded in less than 610 mm. Hence, a 610 mm subgrade layer is considered, such that the box boundary will not influence the stress distribution.

Based on the published literature, the geocell acts like a semi-rigid beam that means the stress is distributed over a wider area. If the box size is restricted to only 915 mm, then it can accommodate only two geocell pockets on each side. If the geocell acts like a beam, then the portion of the load may be absorbed by the box. Hence, this study selected the box dimensions of 1.2 m × 1.5 m, which allowed placement of 3–4 geocell pockets, thus, minimizing the influence of the box boundary.

Materials

In this study, a lower modulus base material is reinforced with a 152 mm high geocell. Subgrade and base materials were obtained from the side of a low-volume road in Texas. The material properties are shown in Table 1 along with the test procedure followed for obtaining material properties. Each pocket of geocell, under stretched conditions, has a longitudinal length of 234 mm, the transversal length of 203 mm, a height of 150 mm, and a thickness of 1 mm. This study used only 101 mm as cover thickness; however, it is necessary to evaluate the required optimum cover thickness above geocell in a future study, as suggested by Tafreshi and Dawson 2010 [1].

Testing, Data Collection, and Refinement

Two samples were prepared one with geocell reinforcement and the other one without any reinforcement. In both samples, the subgrade of 610 mm thickness was placed. In Sample 1 (unreinforced base), the base layer of 254 mm was placed on top of the subgrade. In Sample 2 (geocell-reinforced), a base layer of 152 mm reinforced with the geocell layer is overlaid on top of the subgrade, followed by 101 mm of the cover layer (unreinforced base). Subgrade and base layers are compacted to a minimum of 95% of MDD in 152 mm layers. The compaction was performed using a plate vibrator.

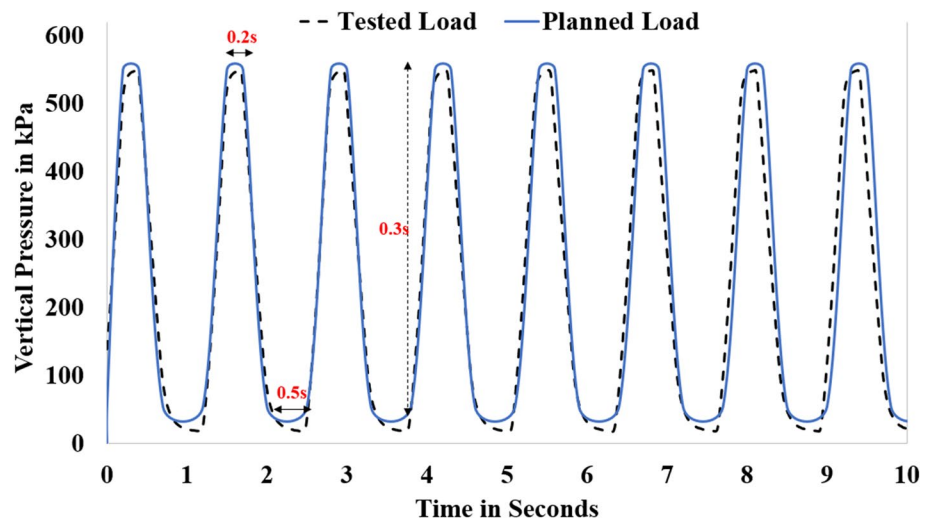
A cyclic loading pattern was applied at the center of the tank using a 305 mm-diameter 25 mm-thick steel plate to replicate the pavement loading (shown in Fig. 2). A 12.5 mm rubber padding was glued to the bottom of the loading plate to simulate the tire flexibility. Ideally, a 0.1 s of loading followed by a rest period of 0.9 s is preferred for simulating traffic loading. However, the loading signal was modified as 0.2 s of loading and 1.0 s of rest due to limitation of the MTS® loading system. Figure 2 shows the planned and achieved loading. In the laboratory evaluation, 20,000 load cycles of 551 kPa, 5000 cycles of 689 kPa, and 5000 cycles of 827 kPa were applied. The tests performed at higher stresses were to evaluate the effectiveness of geocell under high loads.

In this study, the benefits of the geocell reinforcement were estimated by comparing its performance with an unreinforced sample. Pressure cells (230 mm diameter and 6 mm height) and strain gauges were used to monitor the response of the geocell. The stress distribution beneath geocell was evaluated by placing three pressure cells on top of the subgrade (placed at the center below three consecutive geocell pockets), as shown in Fig. 3a. Strain gages were glued and adequately protected to monitor the hoop strains developed in the geocells. 120 Ω strain gages were selected based on its sensitivity as well as its suitability with the data acquisition system. A half-bridge strain gage circuit was selected to enhance the signal-to-noise ratio.

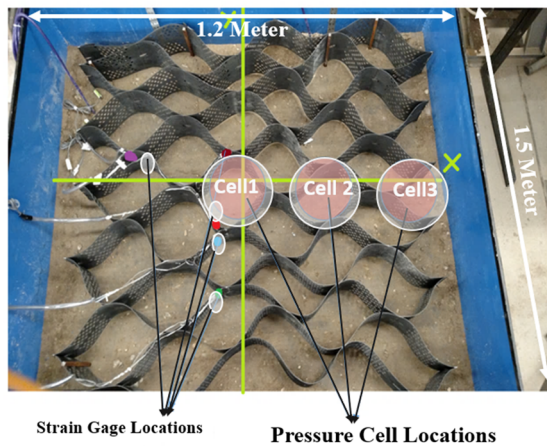
Table 1 Material properties

	Maximum dry-density (MDD) kg/m ³	Optimum moisture content (%)	Plasticity index	Angle of internal friction	Cohesion (kPa)	Resilient modulus (MPa)	Elastic modulus portable seismic pavement analyzer (PSPA) (MPa)
Reference	Tex-114-E		Tex-105-E and Tex-104-E	Tex-117-E		AASHTO T-307	PSPA & SPA Manager Manual 2007
Base	1698	16.7	3	0	60.0	41.4	34.5
Subgrade	2082	6.7	NP	33.8	54.5	34.5	31.0

Fig. 2 Load cycle



(a) Laboratory instrumentation and locations



(b) FEM stress and strain analysis locations

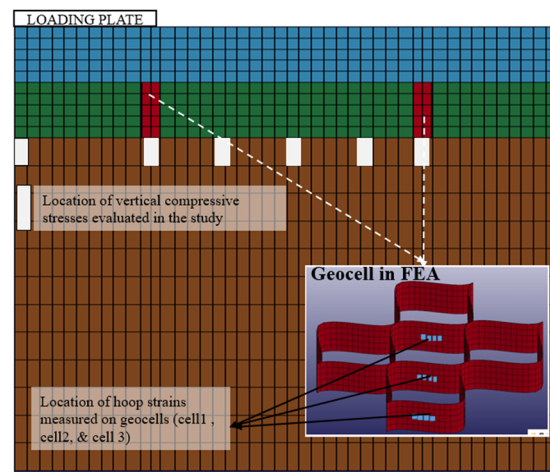


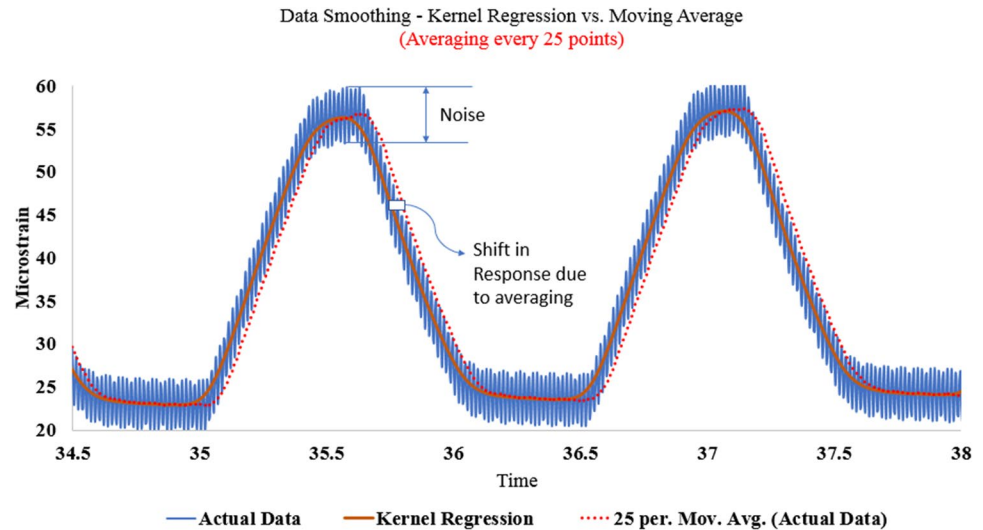
Fig. 3 Laboratory instrumentation locations and FEM stress and strain locations

To collect data from the transducers and loading system, two data acquisition systems were used. The MTS® loading system has a built-in data acquisition system that records the load and vertical deformation on the sample. This data acquisition system can collect data at a frequency of 100 data points/s. The stresses and strains from instrumented sections were recorded through LMS® data acquisition system, which can record 16 locations (strain gages and pressure cells) at a time. The data were acquired at a frequency of 128 data points/s. Before applying the cyclic load on the prepared sample, an initial reading of all electronics was obtained to make sure that the transducers are properly functioning. The initial reading is considered as the datum, and the data collected during the testing are adjusted accordingly.

Since load and deformation transducers generate electronic signals, the transducers tend to measure electronic

noise, as well, which can be cyclic or noncyclic. Since each test is performed for 20,000 load cycles, and each load cycle is around 1.3 s, more than 3 million data points from each channel (strain gages, pressure cells, and load cell) were collected, based on data sampling frequency. Therefore, the data need to be reduced, and noise needs to be minimized without altering the waveform of the applied load (cyclic pulse). In this study, a Kernel regression (nonparametric regression) [30] is used that provides an effective means by which complex displacement/pressure patterns occurring over a wide range of values can be captured. Also, a commonly used moving average method was used for data reduction. Kernel smoothing utilizes locally weighted averages of the data defined by a Kernel. The reduced data are summarized in Fig. 4 using two methods, and the results suggest that the moving average shifts not only the waveform, it is also inefficient in reducing the data points.

Fig. 4 Reduction of data and noise removal using kernel regression



Finite-Element Modeling (FEM)

A three-dimensional FEM was developed to simulate the behavior of reinforced pavement layers and for comparison with the laboratory test results. To perform FEM, a commercially available finite-element program LS-DYNA was selected, because this program allows dynamic FEM and includes a wide list of material and contact models/algorithms. Moreover, the program can also be installed on the High-Performance Cluster (HPC) that reduces the simulation time. Although FEM can identify the level of reinforcement provided by the geocell, the generation of mesh for FEM is complicated due to several factors like the interaction between geocell and adjacent soil, transfer of load, and confinement provided by the geocell, among others.

Additionally, the modeling of geocell required a significant number of elements and nodes to model the honeycomb shape of geocell [5], which also requires significant computational time. A quarter model was used to reduce the number of elements as conditions of symmetry exist in the finite-element model, as shown in Fig. 1b. Modeling the geocell using a rhomboidal pattern is less complex as opposed to the pseudo-sinusoidal honeycomb pattern and has been used in different studies [15, 26].

Many researchers modeled the geocell and infill material as a composite material using a finite-element or finite-difference methods [10–12, 28]. Some researchers [5, 6, 15, 21, 26] modeled them as a separate material. In the geocell-reinforced base layer, the infill material (linear elastic or plastic) and geocell (elastic) respond differently to loading. Also, the working mechanism of each material is different. Thus, the geocell-reinforced layer is modeled, such that the behavior of infill material and geocell is evaluated separately. In this study, the Federal Highway Administration (FHWA, USA) Soil Constitutive Model was used for modeling base, subgrade, and geocell

pocket infill material. This model is a modified Mohr–Coulomb model available in LS-DYNA that was extended to include excess pore-water effects, strain softening, strain hardening, strain-rate effects, and elements’ deletion [31, 32]. These enhancements to the standard soil material models were made to increase the accuracy, robustness, and ease of use for highway applications. The properties of each material were determined using Tex-117-E Test Procedure for Triaxial Compression for Soil and Base Materials following the recommendations of Reid et al. [32] and Saleh and Edwards [33] for samples collected at different sites. Geocell was modeled as a linear elastic material with a density of 950 kg/m³, Poisson’s ratio of 0.45, and elastic modulus of 414 MPa. It was desired to design the FEM with a reinforced layer that allows the expansion of the geocell panels. For this purpose, boundary conditions were removed just for the geocell-reinforced base layer, while the other layers were restrained from lateral movement. The subgrade bottom is restrained from vertical movement. While evaluating the material constitutive models for simulating the geomaterials, it was found that instability did not occur due to the removal of lateral constraints on the nodes at the edge of the reinforced base layer. Discrete elements were used as a contact type between geocell and adjacent base material. The selection of contact type was presented in detail by Inti et al. [18]. The loading pattern similar to the one shown in Fig. 2 is applied. Instead of using 20,000 load cycles, only 100 cycles were applied, because the responses in the laboratory are almost constant after 100 cycles of the load, thus minimizing computational time.

Results and Discussion

The test results from FEM are included in Figs. 5, 6, and 7, while FEM and laboratory result comparisons are included in Figs. 8 and 9. The influence of higher stress on geocell performance is included in Fig. 10.

The vertical stress distribution contours, observed in unreinforced and geocell-reinforced samples, are shown in Fig. 5. The geocell-reinforced layer facilitated the reduction of vertical stress on the subgrade top by absorbing a portion of applied stress (Fig. 5b), which resulted in lower

stress on subgrade, thus increasing its bearing capacity. The vertical stress along the center of the loading plate is presented in Fig. 6. It is observed that the stress is reduced below the loading from the point geocell-reinforced layer started and its effectiveness increased with depth.

The hoop stresses developed in the geocell (below the loading plate) are shown in Fig. 7. The magnitude of stress on geocell is higher than the applied load, indicating that the geocell is effectively absorbing the applied load. The hoop stress is not constant within the geocell pocket (Fig. 7c) as anticipated. The hoop stress is maximum on the bottom part of the geocell (Fig. 7a) and at the center of the cell rather

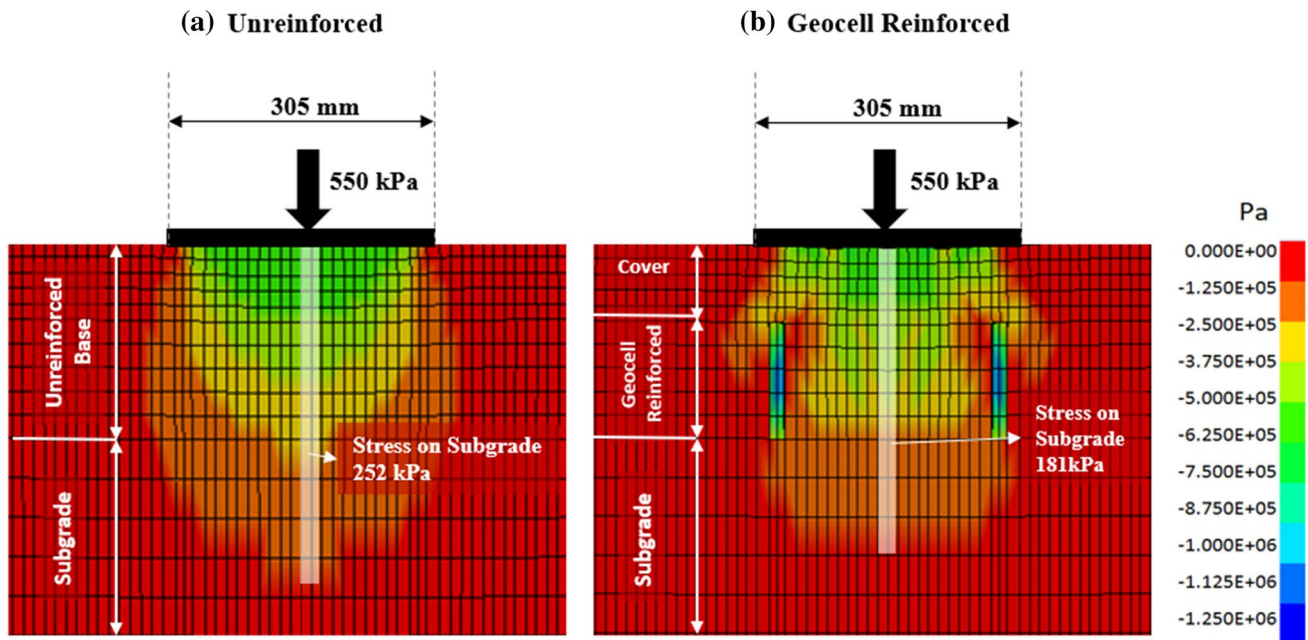
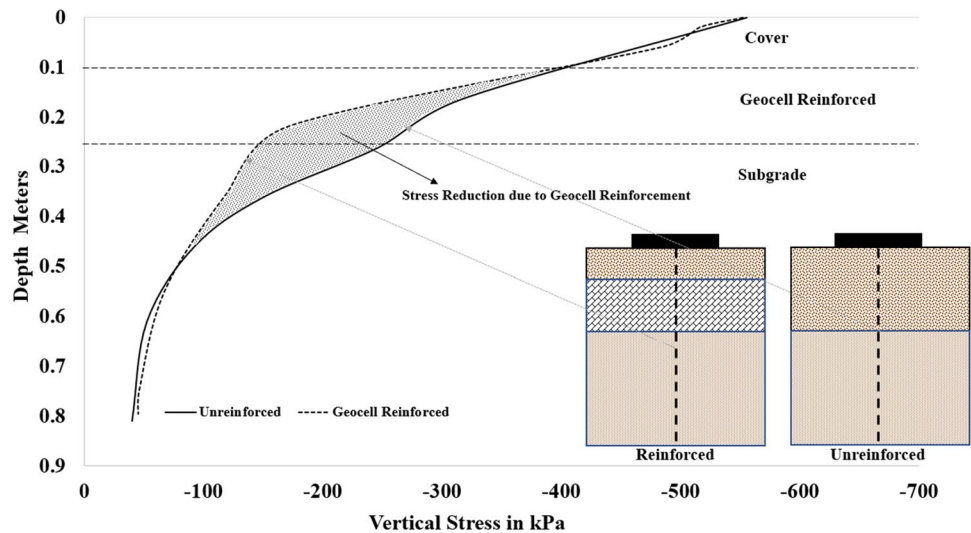


Fig. 5 Vertical stress distribution contours obtained from FEM

Fig. 6 Vertical stress along the depth at the center of loading plate



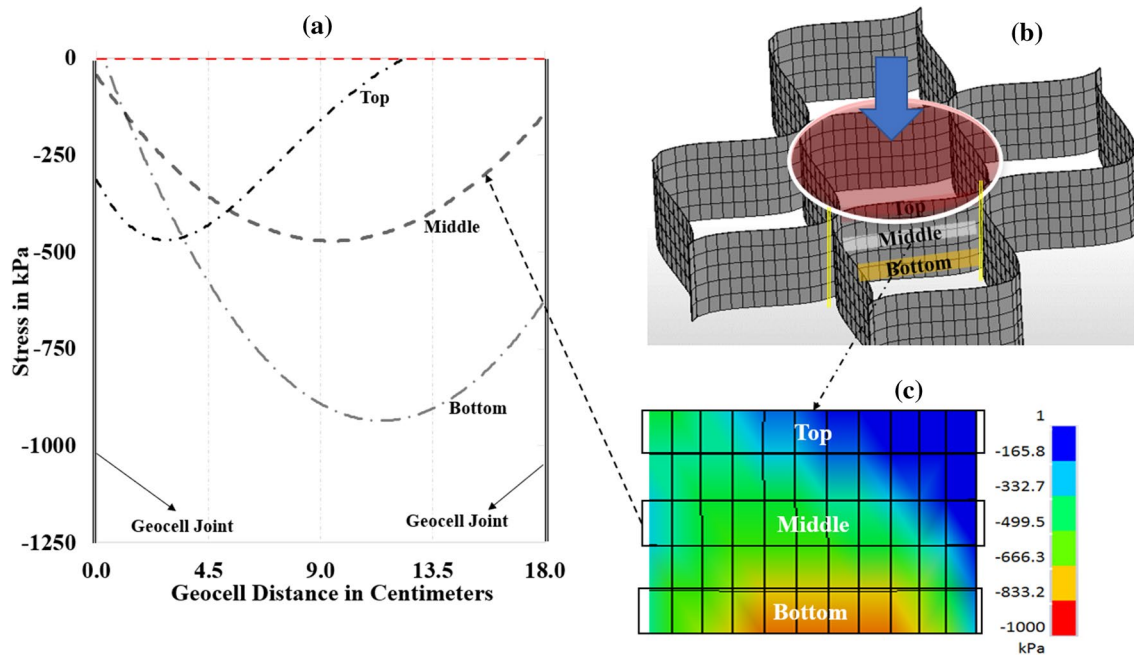


Fig. 7 a Hoop stress on geocell. b Representation of geocell under load. c Hoop stress contours on geocell wall

than at joint, which is often assumed as the weakest spot in the geocell. Similar trends in hoop stress distribution were observed by the study conducted by Saride et al. (2017); however, that study used a monotonic load, whereas this study was performed using a cyclic (repeated) dynamic load. This indicates that the increase in the height of geocell will provide more benefits provided that the infill material is sufficiently compacted with an increase in the height of geocell.

The vertical stresses obtained from the laboratory tests and FEM are shown in Fig. 8. The FEM was calibrated by comparing the stresses with multi-layer model BISAR. The vertical stresses were matched with the stress analysis of the same sections using BISAR and compared with both the laboratory and FEM unreinforced pavement sections. It is visible from Fig. 8a that the BISAR and laboratory results closely matched for unreinforced sections, indicating that the transducers and data analysis are performing as per the theory. The FEM analysis estimated slightly higher stresses in comparison to BISAR estimation. Although higher, the difference in stresses is less than 10%. In both laboratory test results and FEM, the stress on subgrade below the loading plate was reduced by around 69 kPa, which is close to 30%. The stress reduction is much higher outside the loading plate, i.e., after the edge of the loaded geocell pocket. The stress distribution curve of the geocell-reinforced layer neither resembles a flexible pavement nor a rigid pavement but a combination of both.

The hoop strains recorded on the consecutive geocell pockets from the loading plate are shown in Fig. 9. Significant difference in strain values is observed FEM and laboratory. For

instance, the hoop strains observed in first geocell pocket in FEM were 4500 microstrains, whereas the lab testing showed only 1200 microstrains. In FEM, the base material inside geocell is assumed as isotropic and geocell as a linear elastic, which might not be the case in the laboratory sample. It is evident from the strain graphs in Fig. 9a that there is a more elastic recovery in FEM than the laboratory testing. It can be noted that the first geocell pocket below load is taking the considerable load and transferring minimal to the subsequent cells.

The influence of the increase in stresses is summarized in Fig. 10. Geocell is effective in reducing the stresses even when the pavement is subjected to higher loads. This analysis is performed, because often, the low-volume roads are subjected to higher loads due to agricultural equipment movement in Texas. Although the geocell pocket beneath the load plate showed some reduction in stresses on subgrade, the percentage reduction of stresses lessened with increasing load which is contrary to the researcher’s expectation; it is hypothesized through this observation that when geocell is subjected to higher loads, the geocell channelizes the load acting as a conduit, resulting in higher stresses than expected. When greater loads are expected, then using geocell of higher height, multiple layers of geocell or a taller cover over geocell may be required.

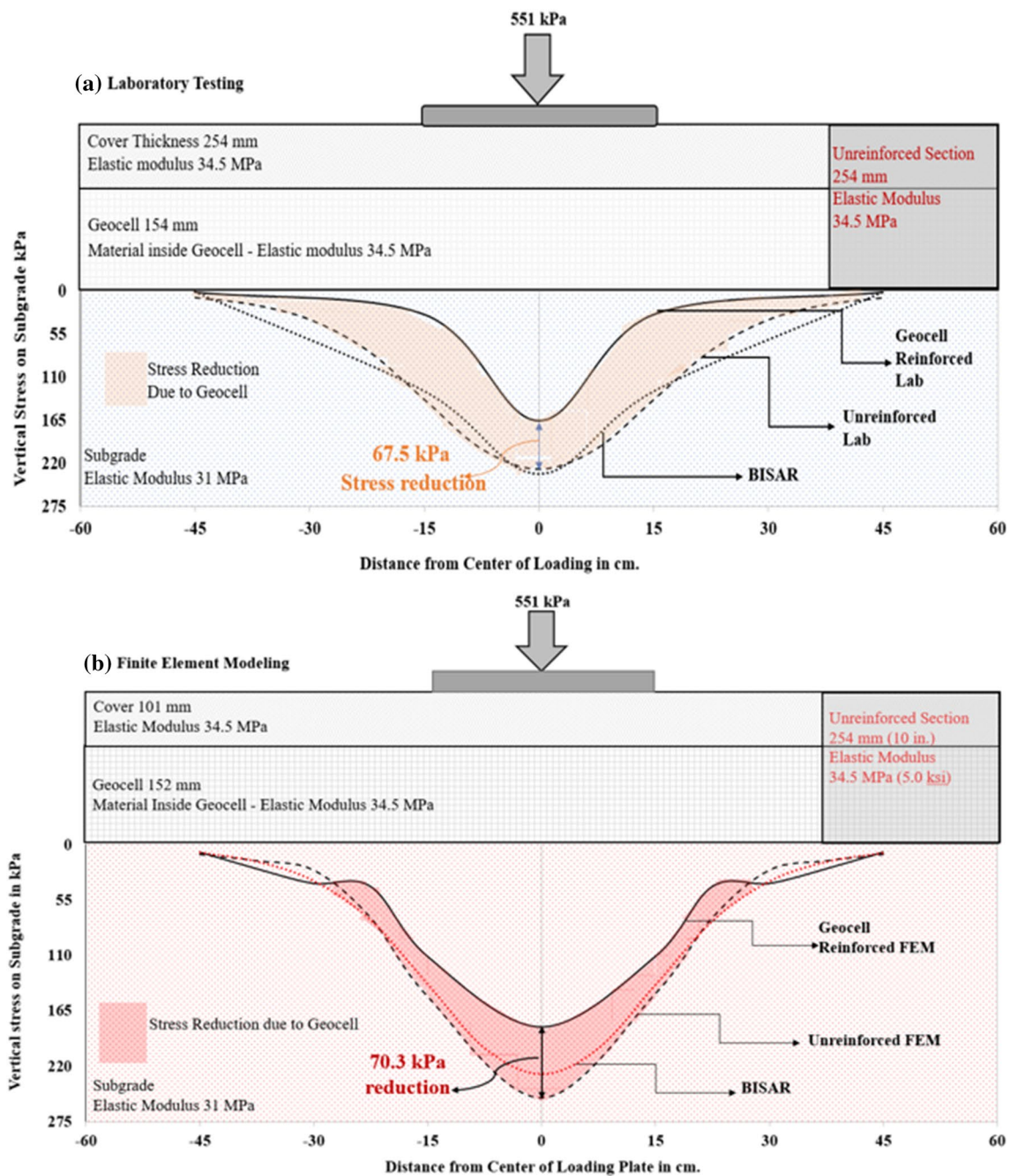


Fig. 8 Vertical stress on subgrade top. a Laboratory. b Finite-element modeling (FEM)

Closure

- This paper presented the laboratory setup, FEM, laboratory data refinement, and analysis of results that can be used for developing a design method for roadways reinforced with geocell.
- The geocell-reinforced layer reduced the vertical stress on the subgrade by acting as a semi-rigid layer. Even

at higher loading pressures of 689 and 827 kPa, the geocell reinforcement worked efficiently.

- Comparison between reinforced and unreinforced sections, in both FEM and laboratory results, indicated that the geocell layer reduced the vertical stress on the subgrade nearly by 30%. However, in this study, only one type of subgrade, base, and geocell are tested. In the future, the study should be expanded by incorporat-

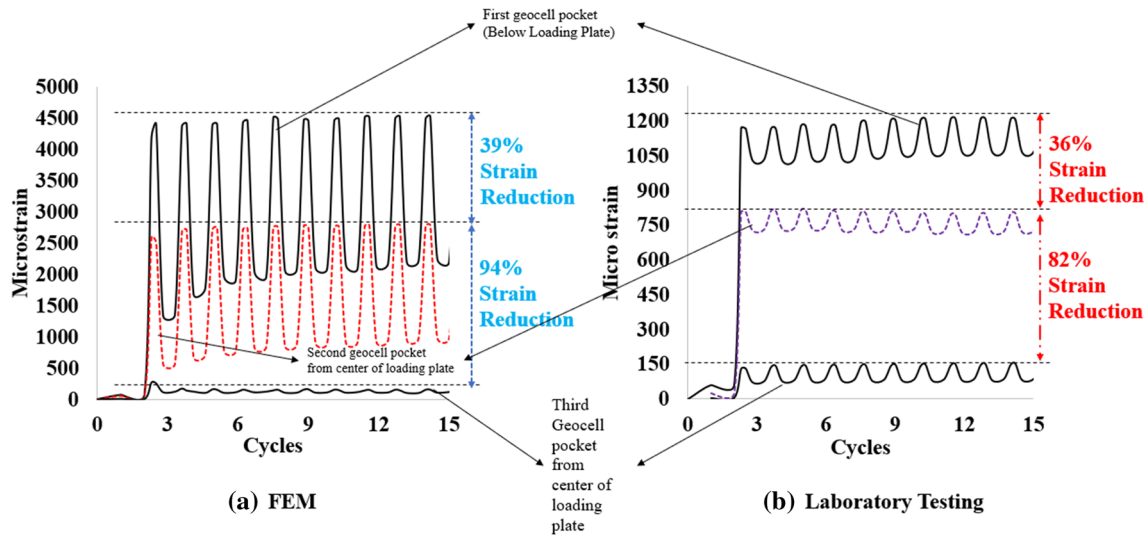


Fig. 9 Strains on the geocell pockets: **a** FEM and **b** laboratory testing

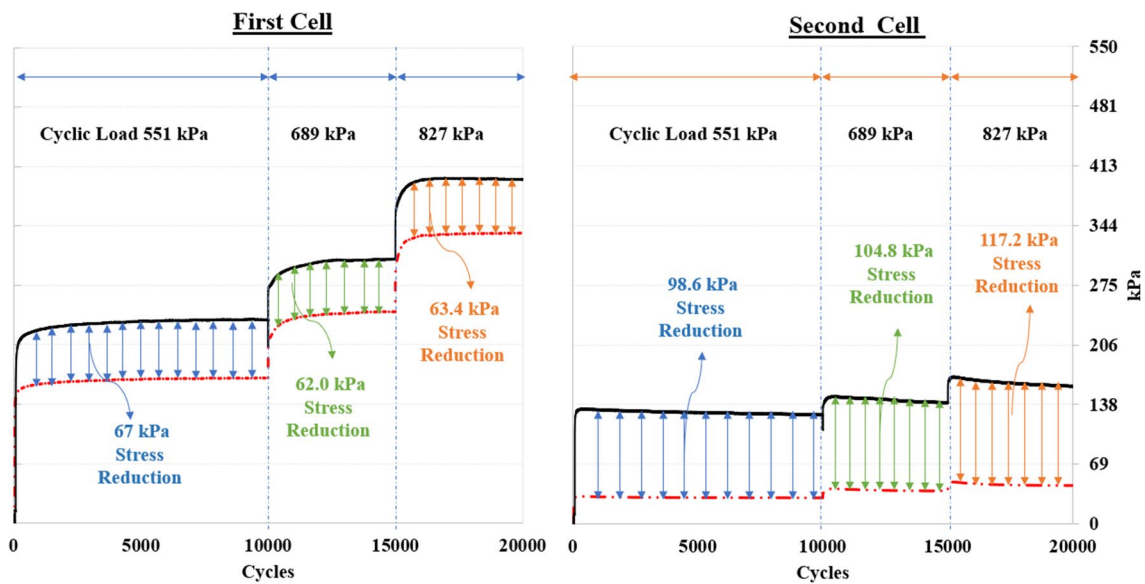


Fig. 10 Performance of geocell at higher loads

ing various combinations of base and subgrade materials and thicknesses.

- Even though the FEM and laboratory test results agree with stress distribution, the FEM model needs further refinement to match the hoop stresses estimated from the laboratory tests.

Acknowledgements The authors like to gratefully acknowledge the financial support for this project received from the Texas Department of Transportation (TxDOT) (Grant no. 0-6833).

References

1. Tafreshi SM, Dawson AR (2010) Behaviour of footings on reinforced sand subjected to repeated loading—Comparing use of 3D and planar geotextile. *Geotext Geomem* 28(5):434–447
2. Maheshwari P, Babu GS (2016) Nonlinear deformation analysis of geocell reinforcement in pavements. *Int J Geomech* 17(6):04016144
3. Mamatha KH, Dinesh SV, Dattatreya JK (2018) Evaluation of flexural behaviour of geosynthetic-reinforced unbound granular material beams. *Road Mater Pavem Des* 20(4):859–876

4. Suku L, Prabhu SS, Ramesh P, Babu GS (2016) Behavior of geocell-reinforced granular base under repeated loading. *Transp Geotech* 9:17–30
5. Hegde A, Sitharam TG (2015) 3-Dimensional numerical modelling of geocell reinforced sand beds. *Geotext Geomem* 43(2):171–181
6. Hegde A, Sitharam TG (2017) Experiment and 3D-numerical studies on soft clay bed reinforced with different types of cellular confinement systems. *Transp Geotech* 10:73–84
7. Biswas A, Krishna AM, Dash SK (2016) Behavior of geosynthetic reinforced soil foundation systems supported on stiff clay subgrade. *Int J Geomech* 16(5):04016007
8. Sireesh S, Faby Mole PA, Madhav MR, Vijay Kumar R (2016) Non-linear response of geocell reinforced dense granular layer over weak soil under circular loading. *Int J Geotech Eng* 10(1):23–30
9. Ghareh S (2015) Numerical modeling of the effect of geocell elements' dimensions on behavior of circular footings. *J Struct Eng Geotech* 5(3):9–14
10. Bathurst RJ, Knight MA (1998) Analysis of geocell reinforced-soil covers over large span conduits. *Comput Geotech* 22(3):205–219
11. Latha GM, Dash SK, Rajagopal K (2009) Numerical simulation of the behavior of geocell reinforced sand in foundations. *Int J Geomech* 9(4):143–152
12. Latha GM, Somwanshi A (2009) Effect of reinforcement form on the bearing capacity of square footings on sand. *Geotext Geomem* 27(6):409–422
13. Satyal SR, Leshchinsky B, Han J, Neupane M (2018) Use of cellular confinement for improved railway performance on soft subgrades. *Geotext Geomem* 46(2):190–205
14. Biabani MM, Indraratna B, Ngo NT (2016) Modelling of geocell-reinforced subballast subjected to cyclic loading. *Geotext Geomem* 44(4):489–503
15. Leshchinsky B, Ling HI (2013) Numerical modeling of behavior of railway ballasted structure with geocell confinement. *Geotext Geomem* 36:33–43
16. Leshchinsky B, Ling H (2012) Effects of geocell confinement on strength and deformation behavior of gravel. *J Geotech Geoenviron Eng* 139(2):340–352
17. Biabani MM, Ngo NT, Indraratna B (2016) Performance evaluation of railway subballast stabilised with geocell based on pull-out testing. *Geotext Geomem* 44(4):579–591
18. Inti S, Sharma M, Tirado C, Tandon V (2015) Base course geocell reinforcement evaluation by comparing 3-D FEM and laboratory evaluation. In: 6th International conference on structural engineering and construction management 2015, Kandy
19. Zhang L, Zhao M, Shi C, Zhao H (2010) Bearing capacity of geocell reinforcement in embankment engineering. *Geotext Geomem* 28(5):475–482
20. Saride S, George AM, Puppala AJ (2017) Experimental and numerical evaluation of reinforcement mechanism of geocells. In: Transportation research board 96th annual meeting 2017, Washington
21. Han J, Pokharel SK, Yang X, Manandhar C, Leshchinsky D, Halahmi I, Parsons RL (2011) Performance of geocell-reinforced RAP bases over weak subgrade under full-scale moving wheel loads. *J Mater Civ Eng* 23(11):1525–1534
22. Pokharel SK et al (2010) Investigation of factors influencing behavior of single geocell-reinforced bases under static loading. *Geotext Geomem* 28(6):570–578
23. Bortz B, Hossain M, Halami I, Gisi A (2012) Accelerated pavement testing of low-volume paved roads with geocell reinforcement. *Advances in pavement design through full-scale accelerated pavement testing*, p 215
24. Emersleben A, Meyer N (2008) Bearing capacity improvement of gravel base layers in road constructions using geocells. *Int Assoc Comput Methods Adv Geomech*
25. Tanyu BF, Aydilek AH, Lau AW, Edil TB, Benson CH (2013) Laboratory evaluation of geocell-reinforced gravel subbase over poor subgrades. *Geosynth Int* 20(2):47–61
26. Yang X, Han J, Pokharel SK, Manandhar C, Parsons RL, Leshchinsky D, Halahmi I (2012) Accelerated pavement testing of unpaved roads with geocell-reinforced sand bases. *Geotext Geomem* 32:95–103
27. Mhaikar SY, Mandal JN (1996) Investigations on soft clay subgrade strengthening using geocells. *Constr Build Mater* 10(4):281–286
28. Pokharel SK (2010) Experimental study on geocell-reinforced base under static and dynamic loading. *Dissertation, University of Kansas*
29. Giroud JP, Han J (2004) Design method for geogrid-reinforced unpaved roads. I. Development of design method. *J Geotech Geoenviron Eng* 130(8):775–786
30. Fan J (1992) Design-adaptive nonparametric regression. *J Am Stat Assoc* 87(420):998–1004
31. Lewis BA (2004) Manual for LS-DYNA soil material model 147 (No. FHWA-HRT-04-095)
32. Reid JD, Coon BA, Lewis BA, Sutherland SH, Murray YD (2004) Evaluation of LS-DYNA soil material model 147 (No. FHWA-HRT-04-094)
33. Saleh M, Edwards L (2011) Application of a soil model in the numerical analysis of landmine interaction with protective structures. In: 26th International symposium
34. PRESTO GEOSYSTEMS “GEOWEB® Load Support System Technical Overview” 670 N Perkins Street, Appleton, Wisconsin, USA 54914. <https://www.prestogeo.com/design/soil-stabilization/geoweb-load-support/>
35. Wang F, Lytton RL (1993) System identification method for back calculating pavement layer properties. *Transp Res Rec* 1384:1–7

Publisher's Note Springer Nature remains neutral with regard to jurisdictional claims in published maps and institutional affiliations.